Towards efficient band structure and effective mass calculations for III-V direct band-gap semiconductors

Yoon-Suk Kim,[*] Martijn Marsman, and Georg Kresse

Department of Computational Materials Physics, University of Vienna, Sensengasse 8/12, A-1090 Vienna, Austria

Fabien Tran and Peter Blaha

Institute of Materials Chemistry, Vienna University of Technology, Getreidemarkt 9/165-TC, A-1060 Vienna, Austria

(Received 26 August 2010; published 24 November 2010)

The band structures and effective masses of III-V semiconductors (InP, InAs, InSb, GaAs, and GaSb) are calculated using the *GW* method, the Heyd, Scuseria, and Ernzerhof hybrid functional, and modified Becke-Johnson combined with the local-density approximation (MBJLDA)—a local potential optimized for the description of the fundamental band gaps [F. Tran and P. Blaha, Phys. Rev. Lett. **102**, 226401 (2009)]. We find that MBJLDA yields an excellent description of the band gaps at high-symmetry points, on par with the hybrid functional and *GW*. However, the effective masses are generally overestimated by 20–30 % using the MBJLDA local multiplicative potential. We believe this to be related to incorrect nearest-neighbor hopping elements, which are little affected by the choice of the local potential. Despite these shortcomings, the MBJLDA method might be a suitable approach for predicting or interpolating the full band dispersion, if only limited experimental data are available. Furthermore, the method is applicable to systems containing several thousand atoms where accurate quasiparticle methods are not applicable.

I. INTRODUCTION

The zinc-blende III-V semiconductors, e.g., InP, InAs, InSb, GaAs, and GaSb, have received considerable attention in the last decades since it has been realized that they have potential to be employed as base materials for light-emitting diodes, infrared detectors, quantum dots, and quantum-well applications.[1–3] Consequently, the materials have been thoroughly investigated experimentally as well as theoretically, paying particular attention to their fundamental properties and band topologies.[4–8] The theoretical calculations are often performed using density-functional theory (DFT) within local (or semilocal) approximations. Although structural properties, such as lattice constants and bulk moduli, are predicted rather well using DFT, it is well established and comes as no surprise that the description of electronic properties, e.g., band gaps and effective masses, is unsatisfactory using conventional ground-state Kohn-Sham DFT. In conventional DFT calculations, both, the exchange energy (E_x) as well as the correlation energy (E_c) are treated by a local or semilocal approximation. Due to self-interaction errors and the lack of an integer discontinuity of the exchange-correlation energy and potential upon changing the number of electrons, the Kohn-Sham one electron band gaps are always too small compared to experimental quasiparticle (QP) band gaps.[9,10] Moreover, for InAs, InSb, and GaSb, the band ordering at the Γ point is incorrect, and, resultantly, the band topologies and effective masses are crossly wrong.[11] Good band topologies and reasonable effective masses are, nevertheless, a prerequisite for modeling nanostructures and electronic devices. In nanostructures, e.g., quantum dots, allowed low-energy states often correspond to slow variations in the phase factor from one unit cell to the next and they are hence mostly determined by the effective masses. Likewise, the behavior of electronic devices is largely determined by the band gap and the curvature of the bands close to the conduction-band minimum (CBM) and valence-band maximum (VBM).

In order to obtain a reasonable description of these properties (QP band gaps and effective masses), the self-energy operator Σ and the corresponding quasiparticle equation need to be determined, for instance, in the widely adopted *GW* approximation.[12,13] Unfortunately, for solids, even the most sophisticated methods presently available—state-of-the-art self-consistent *GW* calculations—fail to predict accurate band gaps and effective masses without empirically adjusting the self-energy operator.[14,15] This seems to be related to the neglect of ladder diagrams that have been proven to be required in the context of self-consistent *GW* calculations in order to obtain accurate screening properties and band gaps.[16,17] Moreover, for unit cells with more than 100 valence electrons, such self-consistent *GW* calculations including ladder diagrams are currently impossible. More efficient, albeit fundamentally less well-founded solutions to the band-gap problem are therefore needed, and recently hybrid functionals have emerged as a possible and convenient option. The first to suggest this approach was Muscat *et al.*, who realized that band gaps are predicted in reasonable agreement with experiment using the B3LYP (Becke-3-Lee-Yang-Parr) hybrid functional.[18] For semiconductors, even better results can be obtained using the hybrid functional proposed by Heyd, Scuseria, and Ernzerhof (HSE) (Ref. 19) as amply demonstrated in the work of Scuseria.[20,21] This was also confirmed by other independent studies,[22,23] including very challenging materials such as lead chalcogenides,[24] ternary and quaternary compounds important for next-generation solar cells,[25] as well as InP, InAs, and InSb.[26]

Even though, hybrid functionals can be applied to reasonably large systems containing several thousand valence electrons, the calculations are still rather expensive, since a

double summation over k points is required to evaluate the Hartree-Fock (HF) exchange.[19] The modeling of large nanostructures with several thousand atoms is therefore certainly out of reach, and even more efficient methods are needed. Ideally these should retain the efficiency of DFT calculations (or even improve upon them). The first such approach goes back to Christensen and Cardona *et al.*[27,28] who suggested to introduce an attractive potential at the atomic cores to shift the valence-band states to lower energies. This allows to increase the band gap resulting in improved effective masses that are crucial for the modeling of nanostructures. Similar ideas were applied by Zunger *et al.*[29–33] The disadvantage of these methods is that they require an extensive fitting to experimental data, which are often scarce and possibly inaccurate. A very elegant approach solving this dilemma has been recently suggested by Tran and Blaha.[34,35] In their MBJLDA method (modified Becke-Johnson combined with the local-density approximation for the correlation), the density functional is modified in such a way that accurate band gaps are predicted.[35–37] In principle, this method is entirely parameter free, however, in the present work a single parameter is adjusted such that the experimental band gap is recovered. The incentive for doing so is that (i) all available methods (including sophisticated *GW* and hybrid functionals) result in band gap errors on the order of 10–20 % for small gap semiconductors, (ii) the band gap has a strong influence on the effective masses, and (iii) fundamental band gaps are usually very accurately known from experiment. If the effective masses and the band topologies are the main target quantities, it seems sensible to adjust the potentials to describe the known experimental values, e.g., the band gap, correctly.

Our aim is to determine how well these optimized local potentials perform in describing the foresaid band topologies and effective masses. If they perform well, the optimized local potential method of Tran and Blaha would be ideally suited to model the *electronic properties* of large nanostructures that are currently out of reach for *GW* or hybrid functional calculations. This would open an important field of applications presently only covered by more semiempirical methods, such as tight-binding approximations or semi-empirical pseudopotential methods. To evaluate the performance of the method, we calculate the band structures of selected III-V semiconductors using *GW*, hybrid functionals and MBJLDA, and compare to experimental values.

II. COMPUTATIONAL DETAILS

A. PAW calculations

Most results of this study were obtained using the Vienna *ab initio* simulation package (VASP).[38] The projector-augmented-wave (PAW) method[39] as implemented in the VASP code[40] was utilized to describe the interaction between the ionic cores and the valence electrons. The generalized gradient approximation (GGA) as parameterized by Perdew, Burke, and Ernzerhof (PBE) (Ref. 41) was employed to describe the exchange-correlation potential in the standard DFT calculations. We have chosen this specific functional because PBE yields slightly larger band gaps than standard LDA (improving agreement with experiment) and because the applied

hybrid functional is based on the PBE functional. In practice, however, results for PBE and LDA are very similar. For Tran's MBJLDA method the MBJ exchange potential is combined with LDA (Ref. 42) for the correlation potential.

The present calculations use scalar-relativistic PAW potentials, where both the core as well as the valence orbitals are treated using a scalar relativistic Hamiltonian. Spin-orbit coupling (SOC) effects are included self-consistently up to second order (*LS* coupling).[43] Since the SOC term is large only close to the core, the corresponding contributions to the Hamiltonian are only evaluated inside the PAW spheres using all-electron partial waves.

The hybrid functionals used in the present work follow the HSE scheme,[19] which employs a screened short-range (SR) HF exchange instead of the full exact HF exchange. The exchange-correlation energy is defined as

$$E_{xc}^{HSE} = E_x^{PBE} - \frac{1}{4}E_x^{PBE,SR}(\mu) + \frac{1}{4}E_x^{HF,SR}(\mu) + E_c^{PBE}, \quad (1)$$

where the screening parameter μ defines the range separation and is usually set to 0.2 Å^{-1} (HSE06 scheme) for both, the HF and the PBE part.[44] $E_x^{PBE,SR}$ is a density functional for the SR part of the exchange energy whereas $E_x^{HF,SR}(\mu)$ is the exact nonlocal exchange evaluated with a screened Coulomb kernel. The interaction range of the SR nonlocal exchange ($\pi/\mu \approx 15$ Å) is over several nearest neighbors and thus considerably longer than the interaction range in conventional semilocal functionals. To allow a fair comparison with the optimized local potentials, which are adjusted to fit the experimental band gap, we also decided to adjust μ such that the experimental band gap is fitted. Results for these calculations will be reported alongside conventional HSE06 calculations and will be referred to as HSE$_{bgfit}$ calculations.

Two "local" band-gap correction schemes were used in the present work. Christensen's approach is a simple procedure that simultaneously corrects the gaps and the band dispersion by introducing "false Darwin shifts," This is done by adding an external local potential to the effective Kohn-Sham potentials.[27] The local potential is of the form

$$V_\omega(r) = V_0 \frac{r_0}{r} \exp[-(r/r_0)^2] \quad (2)$$

at the atomic sites, where r denotes the distance from the nucleus. The range parameters, r_0, are chosen sufficiently small (0.015 a.u.) to affect mainly s-like spherical states. Usually the r_0 values are kept fixed and the V_0 parameters are varied until the gaps are fitted to the experimental values.

Second, Tran's MBJLDA method is applied. The method is a modification of the original Becke and Johnson (BJ) (Ref. 45) method, which was designed to reproduce the shape of the exact exchange optimized effective potentials of atoms. It is used in combination with LDA correlation. The modified BJ exchange potential is

$$V_{x,\sigma}^{MBJ}(\mathbf{r}) = cV_{x,\sigma}^{BR}(\mathbf{r}) + (3c-2)\frac{1}{\pi}\sqrt{\frac{5}{12}}\sqrt{\frac{2\tau_\sigma(\mathbf{r})}{\rho_\sigma(\mathbf{r})}}, \quad (3)$$

where ρ_σ is the electron density, τ_σ is the kinetic-energy density, and

TABLE I. Potential parameters of the projector-augmented-wave method. See text for details.

Element	Valence	R_{core} (a.u.)	E_{cut} (eV)	Local
Ga	$3d^{10}4s^24p^1$	2.3	283	$3f$
In	$4d^{10}5s^25p^1$	2.5	240	$4f$
P	$3s^23p^3$	1.9	255	$3d$
As	$4s^24p^3$	2.1	209	$4f$
Sb	$5s^25p^3$	2.3	173	$5f$

$$V_{x,\sigma}^{BR}(\mathbf{r}) = -\frac{1}{b_\sigma(\mathbf{r})}\left[1 - e^{-x_\sigma(\mathbf{r})} - \frac{1}{2}x_\sigma(\mathbf{r})e^{-x_\sigma(\mathbf{r})}\right] \quad (4)$$

is the Becke and Roussel (BR) potential,[46] which was introduced to mimic the Coulomb potential created by the exchange hole. The function b_σ is calculated via $b_\sigma = [x_\sigma^3 e^{-x_\sigma}/(8\pi\rho_\sigma)]^{1/3}$ and x_σ is determined from the nonlinear one-dimensional equation

$$\frac{x_\sigma e^{-2x_\sigma/3}}{x_\sigma - 2} = \frac{2}{3}\pi^{2/3}\frac{\rho_\sigma^{5/3}}{Q_\sigma}, \quad (5)$$

where

$$Q_\sigma = \frac{1}{6}(\nabla^2\rho_\sigma - 2\gamma D_\sigma) \quad (6)$$

and

$$D_\sigma = 2\tau_\sigma - \frac{1}{4}\frac{(\nabla\rho_\sigma)^2}{\rho_\sigma}. \quad (7)$$

A Newton-Raphson algorithm[47] is used to determine x_σ. The BR and BJ potentials are local and completely determined by ρ_σ, $\nabla\rho_\sigma$, $\nabla^2\rho_\sigma$, and τ_σ.

As we will see later, the c value in Eq. (3) can be determined self-consistently from the average of $\frac{\nabla\rho}{\rho}$ in the unit cell. In the present work, however, the parameter c was adjusted such that the experimental band gaps are reproduced. We note that if an exact reproduction of the experimental band gap is required, a fit of c is necessary.

The parameters of the PAW potentials employed in this work, i.e., the core radii (R_{core}), the energy cutoffs (E_{cut}), and the states treated as valence states, are summarized in Table I. The specific orbitals indicated in the column "Local" in Table I were chosen as local potential for the PAW potential generation. In the present study, the semicore Ga 3d and In 4d states were always treated as valence states.

The parameters of the optimized local potential methods that we employed in this paper are tabulated in Table II. For Christensen's approach, the parameters were obtained by fitting the experimental conduction band minima at Γ, X, and L and the spin-orbit splitting (ΔSO) using a simplex algorithm. For the MBJLDA method (MBJLDA$_{bgfit}$), on the other hand, only the fundamental band gap at the Γ point was fitted to the experiments. Modest variations in the c value between 1.17 and 1.23 were found to be necessary in order to fit the band gaps. For comparison, we also tried to fit the effective

TABLE II. Semiempirical parameters for the band-gap correction methods used in this work. HSE$_{bgfit}$ lists the screening parameter μ that fits the band gap for hybrid functionals. The parameter $V_0^{ion}(r_0^{ion})$ is in units of electron volt (a.u.). Self-consistently obtained c values are listed in the MBJLDA column. The column MBJLDA$_{bgfit}$ lists the optimized c to fit the band gap. The parameters for MBJLDA$_{efmfit}$ fitting the effective masses are given in parentheses.

Material	HSE$_{bgfit}$	Christensen	MBJLDA	MBJLDA$_{bgfit}$
InP	0.22	$V_0^{In}=-2200$ $V_0^{P}=13264$ $r_0^{In}=0.015$ $r_0^{P}=0.015$	1.219	1.170
InAs	0.20	$V_0^{In}=1907$ $V_0^{As}=6500$ $r_0^{In}=0.015$ $r_0^{As}=0.015$	1.229	1.190
InSb	0.23	$V_0^{In}=10700$ $V_0^{Sb}=-145$ $r_0^{In}=0.015$ $r_0^{Sb}=0.015$	1.209	1.200 (1.160)
GaAs	0.12	$V_0^{Ga}=-2813$ $V_0^{As}=11738$ $r_0^{Ga}=0.015$ $r_0^{As}=0.015$	1.231	1.233 (1.120)
GaSb	0.15	$V_0^{Ga}=14106$ $V_0^{Sb}=-300$ $r_0^{Ga}=0.015$ $r_0^{Sb}=0.015$	1.207	1.224

electron mass to the experiments using the c value (referred to as MBJLDA$_{efmfit}$) for InSb and GaAs.

All band structure calculations were performed at the experimental equilibrium lattice constants a_0 at 300 K,[48] i.e., 5.869 Å, 6.058 Å, 6.479 Å, 5.648 Å, and 6.096 Å for InP, InAs, InSb, GaAs, and GaSb, respectively, even though the effective masses, which we compare to in this study, have been measured at low temperature (roughly 4–30 K) by cyclotron resonance and Shubnikov-de Haas experiments. This approximation for the lattice constants seems to be reasonable, since the linear thermal expansion coefficients are negligible (smaller than 5×10^{-5} K^{-1}) for the considered materials.

The Brillouin-zone (BZ) integrations were carried out on Γ-centered k-point meshes using the Gaussian smearing method with a width of 0.05 eV. For the band structure and effective mass calculations, ($6\times6\times6$) k points were used, corresponding to a total of 16 irreducible k points in the first BZ.[49] In order to get accurate results for the band structures including SOC, no symmetry operations were employed, and the full mesh of k points corresponding to 216 k points was used. This is necessary because the magnetization density has generally lower symmetry than the crystal.

The band structures $E(\mathbf{k})$ were computed on a discrete k mesh along high-symmetry directions, i.e., from the BZ cen-

TABLE III. WIEN2K input parameters. The atomic sphere radii R_{MT} and the product of the atomic sphere radii R_{MT} and the plane-wave cut-off parameter K_{max}, as well as the orbitals for which local orbitals (LOs) have been included in the basis set are listed. Note that K_{max}^2 corresponds to the energy cutoff in the PAW calculations.

Element	Valence	R_{MT} (a.u.)	$R_{MT}K_{max}$	LOs
Ga	$3d^{10}4s^24p^1$	2.0	9.0	$3d4s$
In	$4d^{10}5s^25p^1$	2.3	9.0	$4d5s$
P	$3s^23p^3$	2.0	9.0	$3s$
As	$3d^{10}4s^24p^3$	2.0	9.0	$3d4s$
Sb	$4d^{10}5s^25p^3$	2.3	9.0	$4d5s$

ter Γ with the coordinates (0,0,0) to the X point (1.0,0.0,0.0), L point (0.5,0.5,0.5), K point (0.75,0.75,0.00), and W point (1.0,0.0,5.0,0.0) in units of ($2\pi/a$, $2\pi/a$, $2\pi/a$). The effective carrier masses m_e^*, m_{hh}^*, m_{lh}^*, and m_{so}^* were evaluated by fitting the conduction and valence bands to a parabola according to $E = \frac{\hbar^2 k^2}{2m_e m^*}$, where m_e denotes the electron rest mass. A k-point spacing smaller than 0.02 Å^{-1} was found to be required in order to avoid nonparabolic effects.

In the case of our GW calculations, the BZ integrations were performed using $(6 \times 6 \times 6)$ k-point grids for InP, InAs, and InSb and using $(8 \times 8 \times 8)$ for GaAs and GaSb, using more than 140 bands for calculating the quasiparticle energies.

B. FP-APW+lo calculations

For comparison, the self-consistent MBJLDA calculations were also performed using the WIEN2K code[50] which is based on the full-potential (linearized) augmented plane-wave and local orbitals (FP-APW+LO) method. In order to guarantee equivalence between the MBJLDA$_{PAW}$ and MBJLDA$_{FP-APW+LO}$ calculations, the same k meshes for the BZ integration were used. The specific input parameters R_{MT} and $R_{MT}K_{max}$ determining the quality of the basis sets are listed in Table III together with the valence electrons and local orbitals. Similar as described above for the PAW method, SOC is included by solving the radial Dirac equation for the In and Ga core electrons and is evaluated by the second-variation method[51] using scalar relativistic eigenvectors for the valence states.

In the parameter-free MBJLDA calculation, the c value is chosen to be the square root of the average of $\frac{|\nabla\rho|}{\rho}$,

$$c = \alpha + \beta \left[\frac{1}{V_{cell}} \int_{cell} \frac{|\nabla\rho(\mathbf{r}')|}{\rho(\mathbf{r}')} d^3\mathbf{r}' \right]^{1/2}, \quad (8)$$

where α and β are two free parameters and V_{cell} is the volume of the unit cell. The two free parameters were optimized to reproduce the band gap of more than 20 solids (see more details in Ref. 35). Since the VASP code currently dose not allow to calculate the c parameter self-consistently, the c values in MBJLDA were obtained by the WIEN2K code, the corresponding values are listed in Table II.

III. RESULTS

A. Band gaps

The fundamental band gaps of III-V semiconductors at the Γ, X, and L points are listed in Table IV. In order to characterize the overall quality of the band dispersion with respect to the experiment, the mean error (ME), mean absolute error (MAE), mean relative error (MRE), and mean absolute relative error (MARE) are listed at the bottom of Table IV. As can be seen the PBE functional yields an underestimation of the band gaps for all materials that we employed in this study. Our results clearly illustrate the problems one is faced with when using a semilocal functional. Whereas for InP and GaAs, PBE predicts a one-electron band gap, the band order is inverted for InAs, InSb, and GaSb at the Γ point, i.e., the anion-p bands are located above the cation-s band. In the present calculations, the error of the available density functionals is usually attributed to shallow cation-d electrons pushing up the anion-p bands (p-d repulsion). The problem can be reduced by treating the d electrons as core electrons, but even then "negative" band gaps are predicted using the PBE functional.

On the other hand, more sophisticated methods than PBE such as GW and HSE06 repair the deficiency and restore the correct band order for InAs, InSb, and GaSb at the Γ point. A simple single-shot G_0W_0 calculation starting from HSE06 wave functions and eigenvalues yields too large band gaps (not shown here, see Ref. 26), since the HSE06 functional predicts too small dielectric constants in the random phase approximation that is usually applied in the GW method.[57,58] The overestimation can be removed by including the electrostatic interaction between electrons and holes in the calculation of the screening properties ϵ (ladder diagram), which enter $W = \epsilon^{-1}v$, where v is the bare Coulomb kernel. The corresponding results, GW test-charge-test-charge calculations, are reported in the column $G_0W_0^{TC\text{-}TC}$. These single-shot $G_0W_0^{TC\text{-}TC}$ calculations were again performed on top of the HSE06 calculations. Since our GW code currently does not allow for a consistent inclusion of SOC, SOC was not included in the calculation of G or ϵ, but the spin-orbit splitting was added *a posteriori* using the spin-orbit corrections obtained for the HSE06 functional. Except for InSb and GaSb, the band gaps of the GW calculations are in quite reasonable agreement with experiment (see Table IV). We believe that the error for InSb and GaSb is mainly related to the neglect of SOC in the determination of ϵ: SOC lowers the split-off band, and raises the heavy-hole and light-hole bands, on average conserving the center of mass. As long as the spin-orbit splitting is small compared to the band gap, it is reasonable to approximate the eigenvalues by the center of mass (i.e., neglecting SOC). But when the spin-orbit splitting approaches the value of the band gap, the influence of SOC on the screening properties cannot be neglected and should be taken into account. A similar observation was already made for PbTe GW calculations.[24] To obtain good agreement with experiment, therefore, SOC should be included in the evaluation of the screening properties, in particular, for the heavier anions, since the hybridization between cation-s and anion-p states increases significantly for heavier atoms,[11,59]

TABLE IV. Energy of the conduction-band minima at the Γ, X, and L points and energy of the valence band maxima at the X and L points evaluated with respect to the valence maximum at the Γ point in units of electron volt. Relativistic effects, e.g., spin-orbit coupling (SOC), are taken into account for all methods. Mean error (ME), mean absolute error (MAE), mean relative error (MRE), and mean absolute relative error (MARE), in the PBE, $G_0W_0^{\text{TC-TC}}$, HSE06, HSE$_{\text{bgfit}}$, Christensen, MBJLDA, and MBJLDA$_{\text{bgfit}}$ band gaps with respect to experiments are also specified. The experimental results are from Ref. 52 (except when noted).

Material	E_g	PBE	$G_0W_0^{\text{TC-TC}}$	HSE06	HSE$_{\text{bgfit}}$	Christensen	MBJLDA[a]	MBJLDA[b]	MBJLDA$_{\text{bgfit}}$ [b]	Expt.
InP	Γ_6^c	0.68	1.32	1.48	1.41	1.43	1.60	1.60	1.42	1.42
	X_6^c	1.73	2.23	2.35	2.31	2.06	2.40	2.47	2.34	2.38
	X_7^v	−2.31	−2.45	−2.52	−2.51	−2.25	−2.15	−2.14	−2.17	−2.20[c]
	L_6^c	1.47	2.15	2.25	2.18	1.80	2.20	2.26	2.11	2.01
	$L_{4,5}^v$	−0.97	−1.02	−1.03	−1.03	−0.92	−0.88	−0.88	−0.89	−1.00[d]
InAs	Γ_6^c	−0.30	0.41	0.42	0.42	0.43	0.61	0.58	0.43	0.42
	X_6^c	1.44	1.75	1.98	1.98	1.65	2.07	2.09	2.01	1.90[e]
	X_7^v	−2.42	−2.58	−2.64	−2.64	−2.39	−2.27	−2.25	−2.27	−2.70[c]
	L_6^c	0.85	1.45	1.53	1.53	1.24	1.54	1.54	1.43	
	$L_{4,5}^v$	−0.97	−1.05	−1.06	−1.06	−0.96	−0.91	−0.90	−0.91	−0.90[d]
InSb	Γ_6^c	−0.38	0.35	0.28	0.24	0.24	0.26	0.28	0.25	0.24
	X_6^c	1.10	1.38	1.53	1.48	1.05	1.54	1.54	1.52	1.80[e]
	X_7^v	−2.43	−2.58	−2.66	−2.64	−2.46	−2.29	−2.29	−2.29	−2.24[d]
	L_6^c	0.32	0.87	0.85	0.81	0.72	0.83	0.84	0.82	0.93
	$L_{4,5}^v$	−1.03	−1.10	−1.12	−1.11	−1.05	−0.97	−0.96	−0.96	−1.05[d]
GaAs	Γ_6^c	0.43	1.51	1.33	1.52	1.54	1.56	1.51	1.52	1.52
	X_6^c	1.34	1.87	1.96	2.15	1.57	1.99	2.00	2.00	2.18[f]
	X_7^v	−2.76	−2.89	−2.99	−3.03	−2.69	−2.61	−2.60	−2.60	−2.80[f]
	L_6^c	0.89	1.74	1.67	1.86	1.40	1.71	1.71	1.72	1.85[f]
	$L_{4,5}^v$	−1.16	−1.22	−1.25	−1.26	−1.12	−1.09	−1.08	−1.08	−1.30[f]
GaSb	Γ_6^c	−0.11	0.85	0.72	0.82	0.88	0.73	0.75	0.82	0.81
	X_6^c	0.67	1.11	1.26	1.36	0.95	1.16	1.17	1.21	1.14
	X_7^v	−2.73	−2.85	−2.95	−2.97	−2.75	−2.60	−2.60	−2.59	−2.72[d]
	L_6^c	0.20	0.84	0.87	0.97	0.78	0.82	0.83	0.87	0.88
	$L_{4,5}^v$	−1.21	−1.27	−1.29	−1.31	−1.23	−1.15	−1.14	−1.14	−1.32[d]
ME (eV)		−0.41	−0.07	−0.07	−0.05	−0.11	0.06	0.07	0.04	
MAE (eV)		0.46	0.12	0.13	0.11	0.18	0.13	0.13	0.10	
MRE (%)		−43.45	−2.44	−3.15	−2.13	−6.13	4.70	5.35	2.30	
MARE (%)		31.70	6.00	5.81	4.40	7.65	4.92	5.12	4.33	

[a]MBJLDA performed using the WIEN2K code.
[b]MBJLDA performed using the VASP code.
[c]Reference 53.
[d]Reference 54.
[e]Reference 55.
[f]Reference 56.

and because spin-orbit splitting within the anion-p shell also increases with increasing anion mass.

For the HSE06 functional with SOC (see Table IV), the band gaps of InAs are practically identical with experiment, whereas those of InP and InSb are overestimated (1.48 eV compared to 1.42 eV; 4% error and 0.28 eV compared to 0.24 eV; 17% error, respectively) and those of GaAs and GaSb are underestimated (1.33 eV compared to 1.52 eV; 13% error and 0.72 eV compared to 0.81 eV; 11% error, respectively). We note that this kind of agreement is typical for the HSE06 functional; with the exception of wide gap insulators, HSE06 predicts very reasonable band gaps fairly

systematically across the periodic table[20–24,26,44] including ternary and quaternary compounds.[25] Fitting the band gap by adjusting the range separation parameter μ is straightforward, and generally improves the position of the CBM and VBM at Γ, X, and L (see the μ values in Table II column HSE$_{\text{bgfit}}$). Consequently, the ME and the MAE for the VBM and CBM are reduced to −0.05 and 0.11, respectively. Christensen's local potential correction method also yields improved agreement with experiment compared to the PBE functional. But in our case, some problems prevail. Particularly, the band gaps at the X and L points are too small. The reason for this is that the CBM state at Γ is localized to some

extent inside the atomic spheres whereas the CBM state at X possesses almost no charge density on the atomic sites, and the L state represents an intermediate case in the zincblende structure.[27,60] This implies that, in order to correct the conduction bands at the X and L points, one needs to add an external potential not only at the atomic site but also in the interstitial region. Christensen overcame this issue by introducing "empty spheres" in the linear-muffin-tin-orbital method. Since empty spheres are not available in our code, which is based on a plane-wave basis set, we lack the correction from the interstitial region required for an accurate description of the X and L points. For GaAs our best fit therefore yields modest results: for Γ_6^c, X_6^c, and L_6^c, our values are 1.54 eV, 1.57 eV, and 1.40 eV whereas Christensen was able to obtain a very good fit to the experiment (1.46 eV, 1.95 eV, and 1.82 eV, respectively[27]). It is obvious that Christensen's approach without empty spheres is not sufficiently accurate. Therefore, we did not consider this method any further.

In order to compare the band-gap errors for the parameter-free hybrid functional (HSE06) and the self-consistent (parameter-free) MBJLDA,[35] MBJLDA calculations were performed using VASP and WIEN2K, where the *c* values were determined from the average of $\frac{\nabla \rho}{\rho}$ in the unit cell. The corresponding values are listed in Table IV (column MBJLDA). The band gaps are on average underestimated by HSE06 and overestimated by MBJLDA, but the MAE for both HSE06 and MBJLDA is similar. From the MBJLDA$_{\mathrm{PAW}}$ and MBJLDA$_{\mathrm{FP\text{-}APW+LO}}$ results, we can confirm the equivalency of the MBJLDA implementation in the VASP and WIEN2K codes.

The MBJLDA$_{\mathrm{bgfit}}$ results are short of astonishing. Overall the agreement for the CBM and VBM at Γ, X, and L is even slightly better than for the HSE$_{\mathrm{bgfit}}$ case, and the ME and MAE drop to 0.04 eV and 0.10 eV. We will return to a more considerate discussion at a later point (Sec. III B).

Even though the HSE$_{\mathrm{bgfit}}$ functional and the MBJLDA$_{\mathrm{bgfit}}$ method lack the fundamental justification of the *GW* method, it is fairly clear that HSE$_{\mathrm{bgfit}}$ and MBJLDA$_{\mathrm{bgfit}}$ are generally yielding the best description, or rather, best *fit* of the band gaps. These calculations are also much less demanding than the sophisticated many-electron calculations (which in the present case would even require vertex corrections in *W*). We have, therefore, limited the following calculations to the HSE$_{\mathrm{bgfit}}$ and the MBJLDA$_{\mathrm{bgfit}}$ method.

Before continuing, we note that for InSb, the experimental CBM at the X point is about 0.25 eV above all theoretical calculations. We believe that the error is mainly in the experimental data for this specific case.[55] Whereas the VBM was accurately determined by angle-resolved photoemission spectroscopy, the CBM at the X and L points are difficult to determine using inverse photoemission spectroscopy. Especially for narrow band gap semiconductors, resonance phenomena may modulate the inverse photoemission intensity in the low-energy range.[55]

B. Band structure

The band structures of the III-V semiconductors were calculated using the HSE$_{\mathrm{bgfit}}$ functional and the MBJLDA$_{\mathrm{bgfit}}$

method, again including SOC. In Fig. 1, the band structures are shown in an energy range from −4 to 3 eV along the important high symmetry lines. As already discussed, the predicted fundamental band gaps are fitted to experiment at the Γ point, and data at the X and L point were not taken into account. The important difference between the hybrid functional and the MBJLDA calculation is that the hybrid functional generally yields a stronger dispersion when moving from Γ to X or L. This is most likely related to a stronger coupling element between the valence anion-*p* band and the conduction band cation-*s* state. HSE predicts excellent values for the VBM at the L point whereas MBJLDA places the VBM at the L point at somewhat too high energies. On the other hand, at the X point the HSE VBM is generally somewhat too low in energy, and now the MBJLDA results are in better agreement with experiment. On average, both functionals seem to perform roughly equally for the valence band dispersion, but as we will see in the next section, the comparison of the effective masses clearly favors the HSE functional, possibly indicating that the experimental values at the X point need careful revision.

For the conduction band, the accuracy of the experimental results is most likely more questionable. HSE yields excellent results for GaAs, which has been extensively measured experimentally. For the other materials, the MBJLDA results look visually somewhat better, but we emphasize again that the experimental determination of the valence band positions at X and L is by no means straightforward.

C. Effective charge-carrier masses

In Table V, the results for the effective electron and hole masses are summarized for the HSE$_{\mathrm{bgfit}}$ functional and the MBJLDA$_{\mathrm{bgfit}}$ method along the direction [100] (Γ to X). For comparison, the experimentally obtained effective masses from Ref. 52 are listed, and the PBE results for InP and GaAs are included as well. The masses were evaluated numerically by fitting the calculated dispersion curves around the Γ point along the directions [100], [110], and [111]. For symmetry reasons, the split-off mass and the electron mass are identical along these directions. The light-hole and heavy-hole effective masses differ along the three direction, but they can be uniquely determined by the three Luttinger parameters γ_i [52,61,62]

$$\left(\frac{m_{hh}^*}{m_e}\right)^{[100]} = \frac{1}{\gamma_1 - 2\gamma_2},$$

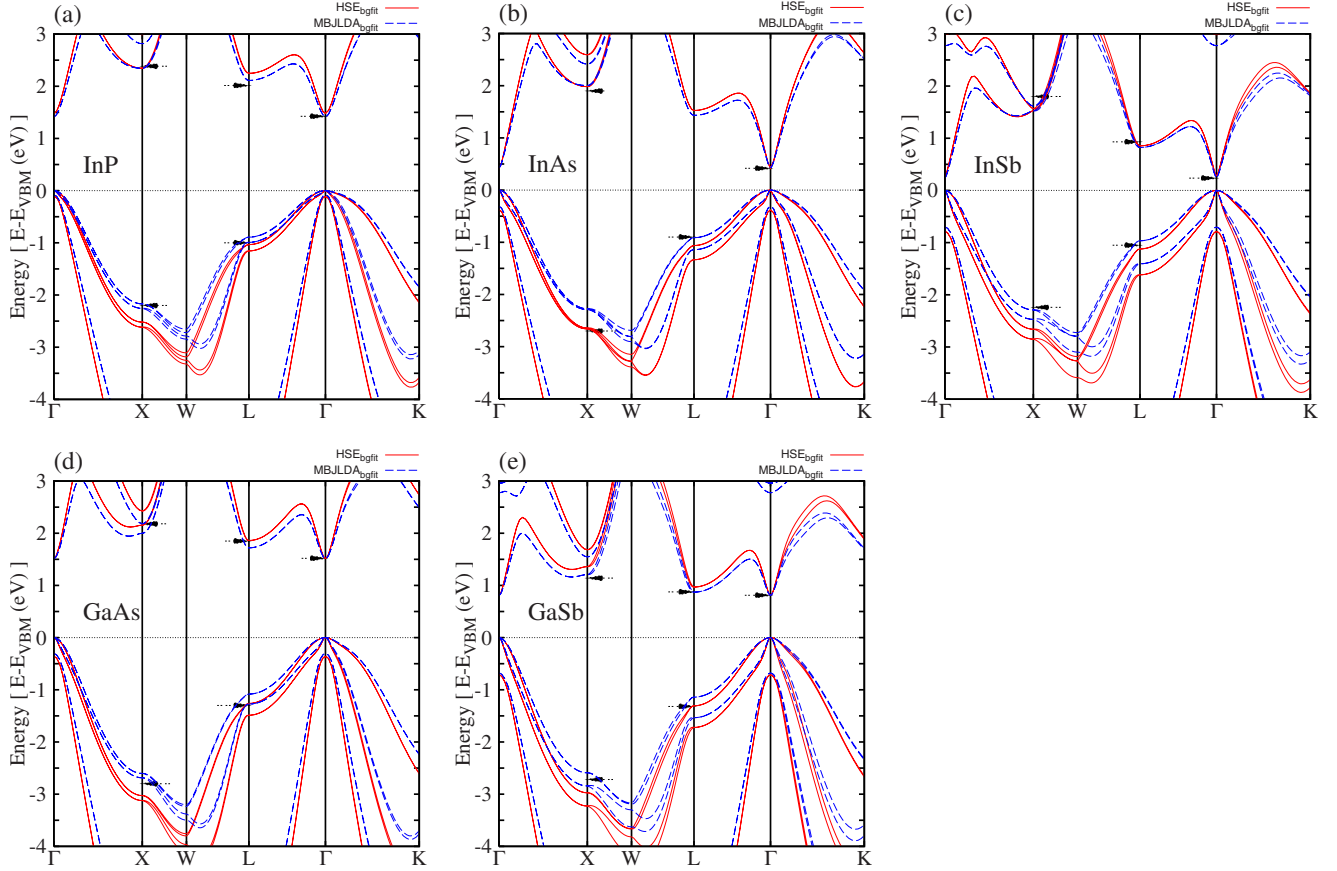$$\left(\frac{m_{hh}^*}{m_e}\right)^{[110]} = \frac{2}{2\gamma_1 - \gamma_2 - 3\gamma_3},$$

$$\left(\frac{m_{hh}^*}{m_e}\right)^{[111]} = \frac{1}{\gamma_1 - 2\gamma_3},$$

$$\left(\frac{m_{lh}^*}{m_e}\right)^{[100]} = \frac{1}{\gamma_1 + 2\gamma_2},$$

$$\left(\frac{m_{lh}^*}{m_e}\right)^{[110]} = \frac{2}{2\gamma_1 + \gamma_2 + 3\gamma_3},$$

FIG. 1. (Color online) The band structures of (a) InP, (b) InAs, (c) InSb, (d) GaAs, and (e) GaSb along Γ-X-W-L-Γ-K obtained from HSE_{bgfit} (solid line) and $MBJLDA_{bgfit}$ (dashed line) calculations (including SOC). The arrows indicate the experimental value.

$$\left(\frac{m_{lh}^*}{m_e}\right)^{[111]} = \frac{1}{\gamma_1 + 2\gamma_3}. \qquad (9)$$

The Luttinger parameters were obtained by a least square fit of the effective hole masses along the three directions and are presented in Table VI. For the HSE_{bgfit} functional ($MBJLDA_{bgfit}$ method), the MAE of the Luttinger parameters (dimensionless) were 0.09(0.39), 2.28(4.78), 3.58(8.26), 0.28(0.75), and 0.56(2.15) for InP, InAs, InSb, GaAs, and GaSb, respectively. In the effective mass fitted MBJLDA ($MBJLDA_{efmfit}$), the MAE was 1.03 and 0.32 as for InSb and GaAs. Recalculating the effective masses from the Luttinger parameters gave results within 0.05 of those reported in Table V. This shows that the present results are numerically accurate, although systematic errors introduced by the functional are another matter.

The electron and light-hole effective masses of PBE show an underestimation of 30–60 % for InP and GaAs, whereas $MBJLDA_{bgfit}$ overestimates the effective electron masses by about 30–50 % with respect to experiment. For HSE_{bgfit}, the agreement with experiments is best, typically better than 10–20 %.

IV. DISCUSSION

Overall, the present study suggests that HSE yields a very good description of the band topology of III-V semiconduc-tors, whereas MBJLDA has troubles reproducing effective masses. Nevertheless, for the effective mass and band-gap results some details remain puzzling, and we feel that only a careful reexamination of the experimental results, beyond the scope of this work, can resolve all issues.

A. Effective masses

Let us start with the effective masses. Among the methods we have employed for calculating the effective masses, the hybrid functional clearly shows the best performance. Comparison is most easily done for the Luttinger parameters (Table VI) and the effective electron mass $m_{electron}^*$ (Table V). We find excellent agreement for the materials with a larger gap but admittedly agreement becomes worse with increasing mass and decreasing band gap. For InSb, errors are largest, on the order of 20%.

The local potential correction method, on the other hand, consistently underestimates the Luttinger parameters and overestimates the effective electron mass ($m_{electron}^*$). Compared to experiment the errors are fairly large amounting to about 20% for the light elements and 40% for InSb and GaSb. This is certainly unsatisfactory. To understand this issue, we have included the effective masses and the Luttinger parameters for PBE for InP and GaAs. The band dispersion around the Γ point is mainly driven by the interaction between the anion-p (VBM) and cation-s band (CBM), which

TABLE V. Effective hole and electron masses at the Γ point in units of the electron rest mass m_e calculated along the ΓX [100] direction using the HSE$_{\text{bgfit}}$ functional and MBJLDA$_{\text{bgfit}}$ taking into account spin-orbit coupling. For comparison, the effective masses for the PBE functional are also listed for InP and GaAs. The experimental values were calculated from the Luttinger parameters tabulated in Ref. 52.

Element	Method	$|m^*_{\text{split-off}}/m_e|$	$|m^*_{\text{light-hole}}/m_e|$	$|m^*_{\text{heavy-hole}}/m_e|$	$|m^*_{\text{electron}}/m_e|$
InP	PBE	0.139	0.073	0.435	0.054
	MBJLDA$_{\text{bgfit}}$	0.230	0.143	0.493	0.108
	HSE$_{\text{bgfit}}$	0.212	0.117	0.479	0.085
	Expt.	0.210	0.121	0.531	0.080
InAs	MBJLDA$_{\text{bgfit}}$	0.133	0.044	0.407	0.036
	HSE$_{\text{bgfit}}$	0.112	0.033	0.343	0.027
	Expt.	0.140	0.027	0.333	0.026
InSb	MBJLDA$_{\text{bgfit}}$	0.150	0.024	0.292	0.022
	MBJLDA$_{\text{efmfit}}$	0.135	0.015	0.287	0.014
	HSE$_{\text{bgfit}}$	0.129	0.018	0.245	0.017
	Expt.	0.110	0.015	0.263	0.014
GaAs	PBE	0.108	0.036	0.320	0.030
	MBJLDA$_{\text{bgfit}}$	0.210	0.112	0.372	0.090
	MBJLDA$_{\text{efmfit}}$	0.173	0.083	0.355	0.066
	HSE$_{\text{bgfit}}$	0.166	0.085	0.314	0.067
	Expt.	0.172	0.090	0.350	0.067
GaSb	MBJLDA$_{\text{bgfit}}$	0.175	0.060	0.267	0.054
	HSE$_{\text{bgfit}}$	0.143	0.047	0.235	0.042
	Expt.	0.120	0.044	0.250	0.039

is symmetry forbidden at Γ (see Sec. IV B). If the interactions were identical for PBE and MBJLDA, one would expect the masses to be proportional to the band gap. This is indeed observed for the electron mass of InP and GaAs. The value $m^*_e(\text{PBE})\frac{E_g(\text{MBJLDA})}{E_g(\text{PBE})}$ yields a good approximation of the electron masses for the MBJLDA$_{\text{bgfit}}$ functional (0.112 for InP and 0.106 for GaAs). Furthermore the MBJLDA$_{\text{bgfit}}$ Luttinger parameters are well approximated by the equation

$$\gamma(\text{MBJLDA}) = \gamma(\text{PBE})\frac{E_g(\text{PBE})}{E_g(\text{MBJLDA})}. \quad (10)$$

Hence, the overestimation of the effective masses using MBJLDA is most likely related to an incorrect description of the coupling element between anion-p and cation-s states. This interaction is mainly determined by the hopping probability from the anion-p states to neighboring cation-s states, i.e., a two center term. In hindsight, it is not astonishing that MBJLDA fails to modify this interaction, since MBJLDA is a purely local correction, which will mainly influence the one-center terms responsible for the energy separation between anion-p and cation-s states. The hybrid functionals are more successful in this aspect. Inclusion of the nonlocal exchange interaction significantly modifies the two center integrals, i.e., the hopping probability between sites. We believe that this is the main reason why the effective masses are better described using hybrid functionals.

Since the masses scale inverse proportional to the band gap, it is also possible to fit the effective masses *instead* of the band gap. The rows marked with MBJLDA$_{\text{efmfit}}$ show the corresponding results for InSb and GaAs. In this case, we only fitted the conduction band mass m^*_{electron} but the Luttinger parameters are also found to agree well with experiment. Unfortunately fitting the effective masses yields too small band gaps of 0.11 eV and 1.07 eV for InSb and GaAs. It is therefore impossible to fit the effective mass and the band gap simultaneously. But from a practical point of view, the proper description of effective masses might be often more relevant than the description of the band gap since effective masses determine which bands are allowed in nanostructures with confinement effects.

B. Valence-band maxima (VBM)

The second important issue is the position of the VBM at the X and L point. Inspection of Fig. 1 and Table IV suggests that MBJLDA$_{\text{bgfit}}$ does a decent job for this, in fact, on par with HSE$_{\text{bgfit}}$. Specifically, the mean errors for the VBM are -0.13 and 0.13 for HSE$_{\text{bgfit}}$ and MBJLDA$_{\text{bgfit}}$, respectively. As we have already discussed, the VBM lies at lower energies for HSE than for MBJLDA, and HSE deviates from experiment dominantly at the X point. Two issues, however, shed doubt on this observation: the *GW* VBM results are very close to the HSE$_{\text{bgfit}}$ results, and the effective masses were better described using HSE. Since the band dispersion along Γ-X is again mostly determined by the two center anion-p cation-s hopping integrals, it seems difficult to rec-

TABLE VI. Luttinger parameters of III-V semiconductors. The values were determined by a least-squares fit to the effective masses along the ΓX [100], ΓL [111], and ΓK [110] directions. The experimental Luttinger parameters are from Ref. 52.

Element	Method	γ_1	γ_2	γ_3
InP	PBE	8.01	2.91	3.49
	MBJLDA$_{bgfit}$	4.53	1.28	1.80
	HSE$_{bgfit}$	5.27	1.63	2.14
	Expt.	5.08	1.60	2.10
InAs	MBJLDA$_{bgfit}$	12.53	5.10	5.73
	HSE$_{bgfit}$	16.50	6.77	7.64
	Expt.	20.00	8.50	9.20
InSb	MBJLDA$_{bgfit}$	22.26	9.47	10.31
	MBJLDA$_{efmfit}$	36.13	16.49	17.27
	HSE$_{bgfit}$	29.44	12.79	13.85
	Expt.	34.80	15.50	16.50
GaAs	PBE	15.29	6.16	6.96
	MBJLDA$_{bgfit}$	5.79	1.60	2.32
	MBJLDA$_{efmfit}$	7.45	2.37	3.12
	HSE$_{bgfit}$	7.51	2.22	3.07
	Expt.	6.98	2.06	2.93
GaSb	MBJLDA$_{bgfit}$	10.13	3.27	4.26
	HSE$_{bgfit}$	12.69	4.31	5.43
	Expt.	13.40	4.70	6.00

oncile the *experimental* effective masses with the *experimental* positions for the VBM at the X point (see also Fig. 1). Either the experiments are in error at the X point, or hybrid functionals and *GW* underestimate the non parabolicity of the bands along Γ-X.

C. Conduction-band minima (CBM)

For the CBM the situation is more concise. HSE$_{bgfit}$ and MBJLDA$_{bgfit}$ yield a similarly good description, most likely both within the experimental error bars. The only disconcerting observation is that our *GW* calculations predict a too small value for X_6^c (typical error 200 meV), and a slightly too small value for L_6^c (typical error 100 meV). For InAs and GaAs, recent self-consistent *GW* calculations by Kotani and Schilfgaarde show a similar problem,[63] as long as the self-energy operator was not empirically adjusted: in their work the dispersion along Γ-X was 0.31 eV for GaAs and 1.42 eV for InAs, close to our values of 0.36 eV and 1.34 eV. The experimental values are clearly larger and very well described by HSE$_{bgfit}$ and MBJLDA$_{bgfit}$. This demonstrates that the *GW* results, despite the fundamental justification of the method, need to be considered with care and on their own do not constitute a sufficient and valid benchmark.

V. CONCLUSIONS

In this paper, the band gaps and effective masses of zinc-blende III-V semiconductors were calculated using the screened hybrid functional (HSE$_{bgfit}$) and the optimized local

potential method (MBJLDA$_{bgfit}$). Before discussing the results in detail, we want to emphasize a few points regarding the MBJLDA functional. (i) The functional uses a purely local multiplicative potential, similar to the Kohn-Sham potential. (ii) However, the MBJLDA potential is *not* an "improved" approximation to the true Kohn-Sham potential. It has been established that the true Kohn-Sham potential is quite close to the LDA or GGA potential for solids; for instance, the Sham-Schlüter potential calculated within the random-phase approximation yields similar one-electron band gaps as the LDA/GGA.[64–66] (iii) Hence, MBJLDA must be regarded as an empirical approach yielding one-electron band gaps in reasonable agreement with the measured QP energies. Not more, but also not less. If the approach predicts good band topologies, it would be ideally suited to calculate the *electronic properties* of large nanostructures, where confinement effects and band folding effects are often the crucial issues.

Using MBJLDA$_{bgfit}$ we found that the energies of the CBM and VBM at the Γ, X, and L points are very well described, certainly on par with the much more expensive hybrid functional HSE$_{bgfit}$, despite the fact that we have fitted the experimental band gap by adjusting the screening parameter in the HSE$_{bgfit}$ functional. In this respect, the MBJLDA$_{bgfit}$ results are indeed very impressive.

Nevertheless, problematic issues remain. The MBJLDA$_{bgfit}$ electron mass for the conduction band is consistently 20% too large. Hybrid functionals perform much better, yielding values within a few percent of experiment (with the exception of InSb). The topology of the valence bands, described by the three Luttinger parameters, is also best accounted for by the hybrid functional, with errors being again largest for InSb. Since the Luttinger parameters are inverse proportional to the effective conduction-band masses, the MBJLDA functional underestimates the Luttinger parameters, with the errors typically amounting to 20–30 % (InSb being again an exception). Unfortunately the effective masses are among the most important properties, for the proper description of QP energies in nanostructures. As we have already emphasized in Sec. I, low-energy states correspond to slow variations in the phase factor from one unit cell to the next and they are mostly determined by the effective mass (particle in a box picture). Hence, accurate predictions of the electronic properties of nanostructures will be difficult using the MBJLDA functional. A possible solution to this problem is to fit the masses instead of the band gaps, which we have demonstrated to be possible.

In hindsight, the present results are certainly not astonishing. The MBJLDA functional is a purely local correction to the Kohn-Sham potential. It essentially modifies the one-center terms but should affect the two center terms very little. Two center terms are obviously important for the description of effective masses. However, one has to keep in mind that it achieves remarkably good overall band topologies, despite the fact that only a single parameter was adjusted. In this respect, the MBJLDA functional clearly supersedes all semiempirical approaches used in the past. Nevertheless, to obtain correct effective masses, corrections beyond a purely local potential will be ultimately required.

*yoon-suk.kim@univie.ac.at; http://cms.mpi.univie.ac.at/

[1] D. E. Aspnes and A. A. Studna, Phys. Rev. B **27**, 985 (1983).

[2] B. R. Bennett and R. A. Soref, IEEE J. Quantum Electron. **23**, 2159 (1987).

[3] M. Razeghi, Nature (London) **369**, 631 (1994).

[4] J. R. Chelikowsky and M. L. Cohen, Phys. Rev. B **14**, 556 (1976).

[5] D. J. Chadi, Phys. Rev. B **16**, 790 (1977).

[6] K. J. Chang, S. Froyen, and M. L. Cohen, Solid State Commun. **50**, 105 (1984).

[7] I. Gorczyca, N. E. Christensen, and M. Alouani, Phys. Rev. B **39**, 7705 (1989).

[8] C. B. Geller, W. Wolf, S. Picozzi, A. Continenza, R. Asahi, W. Mannstadt, A. J. Freeman, and E. Wimmer, Appl. Phys. Lett. **79**, 368 (2001).

[9] R. O. Jones and O. Gunnarsson, Rev. Mod. Phys. **61**, 689 (1989).

[10] P. Mori-Sánchez, A. J. Cohen, and W. T. Yang, Phys. Rev. Lett. **100**, 146401 (2008).

[11] S. Massidda, A. Continenza, A. J. Freeman, T. M. de Pascale, F. Meloni, and M. Serra, Phys. Rev. B **41**, 12079 (1990).

[12] M. S. Hybertsen and S. G. Louie, Phys. Rev. B **34**, 5390 (1986).

[13] X. Zhu and S. G. Louie, Phys. Rev. B **43**, 14142 (1991).

[14] T. Kotani and M. van Schilfgaarde, Solid State Commun. **121**, 461 (2002).

[15] A. N. Chantis, M. van Schilfgaarde, and T. Kotani, Phys. Rev. Lett. **96**, 086405 (2006).

[16] M. Shishkin and G. Kresse, Phys. Rev. B **74**, 035101 (2006).

[17] M. Shishkin, M. Marsman, and G. Kresse, Phys. Rev. Lett. **99**, 246403 (2007).

[18] J. Muscat, A. Wander, and N. M. Harrison, Chem. Phys. Lett. **342**, 397 (2001).

[19] J. Heyd, G. E. Scuseria, and M. Ernzerhof, J. Chem. Phys. **118**, 8207 (2003).

[20] J. Heyd, J. E. Peralta, G. E. Scuseria, and R. L. Martin, J. Chem. Phys. **123**, 174101 (2005).

[21] J. E. Peralta, J. Heyd, G. E. Scuseria, and R. L. Martin, Phys. Rev. B **74**, 073101 (2006).

[22] J. Paier, M. Marsman, K. Hummer, G. Kresse, I. C. Gerber, and J. G. Ángán, J. Chem. Phys. **124**, 154709 (2006).

[23] J. Paier, M. Marsman, K. Hummer, G. Kresse, I. C. Gerber, and J. G. Ángán, J. Chem. Phys. **125**, 249901 (2006).

[24] K. Hummer, A. Grüneis, and G. Kresse, Phys. Rev. B **75**, 195211 (2007).

[25] J. Paier, R. Asahi, A. Nagoya, and G. Kresse, Phys. Rev. B **79**, 115126 (2009).

[26] Y.-S. Kim, K. Hummer, and G. Kresse, Phys. Rev. B **80**, 035203 (2009).

[27] N. E. Christensen, Phys. Rev. B **30**, 5753 (1984).

[28] M. Cardona, N. E. Christensen, and G. Fasol, Phys. Rev. B **38**, 1806 (1988).

[29] L. W. Wang and A. Zunger, Phys. Rev. B **51**, 17398 (1995).

[30] H. Fu and A. Zunger, Phys. Rev. B **55**, 1642 (1997).

[31] A. J. Williamson and A. Zunger, Phys. Rev. B **59**, 15819 (1999).

[32] S. Lany, H. Raebiger, and A. Zunger, Phys. Rev. B **77**, 241201(R) (2008).

[33] S. Lany and A. Zunger, Modell. Simul. Mater. Sci. Eng. **17**, 084002 (2009).

[34] F. Tran, P. Blaha, and K. Schwarz, J. Phys.: Condens. Matter **19**, 196208 (2007).

[35] F. Tran and P. Blaha, Phys. Rev. Lett. **102**, 226401 (2009).

[36] D. J. Singh, Phys. Rev. B **82**, 205102 (2010).

[37] D. J. Singh, Phys. Rev. B **82**, 155145 (2010).

[38] G. Kresse and J. Furthmüller, Comput. Mater. Sci. **6**, 15 (1996).

[39] P. E. Blöchl, Phys. Rev. B **50**, 17953 (1994).

[40] G. Kresse and D. Joubert, Phys. Rev. B **59**, 1758 (1999).

[41] J. P. Perdew, K. Burke, and M. Ernzerhof, Phys. Rev. Lett. **77**, 3865 (1996).

[42] J. P. Perdew and A. Zunger, Phys. Rev. B **23**, 5048 (1981).

[43] R. J. Elliott, Phys. Rev. **96**, 266 (1954).

[44] A. V. Krukau, O. A. Vydrov, A. F. Izmaylov, and G. E. Scuseria, J. Chem. Phys. **125**, 224106 (2006).

[45] A. D. Becke and E. R. Johnson, J. Chem. Phys. **124**, 221101 (2006).

[46] A. D. Becke and M. R. Roussel, Phys. Rev. A **39**, 3761 (1989).

[47] W. H. Press, B. P. Flannery, S. A. Teukolsky, and W. T. Vetterling, *Numerical Recipes: The Art of Scientific Computing* (Cambridge University Press, Cambridge, England, 1986).

[48] O. Madelung, U. Rössler, and M. Schulz, *Condensed Matter: Group IV Elements, IV-IV and III-V Compounds*, Landolt-Börnstein New Series, Group III, Vol. 41A1b, Pt. B, (Springer-Verlag, Berlin, 2002).

[49] H. J. Monkhorst and J. D. Pack, Phys. Rev. B **13**, 5188 (1976).

[50] P. Blaha, K. Schwarz, G. K. H. Madsen, D. Kvasnicka, and J. Luitz, *WIEN2K: An Augmented Plane Wave + Local Orbital Program for Calculating Crystal Properties*, edited by K. Schwarz (Vienna University of Technology, Austria, 2001).

[51] D. D. Koelling and B. N. Harmon, J. Phys. C **10**, 3107 (1977).

[52] I. Vurgaftman, J. R. Meyer, and L. R. Ram-Mohan, J. Appl. Phys. **89**, 5815 (2001).

[53] G. P. Williams, F. Cerrina, G. J. Lapeyre, J. R. Anderson, R. J. Smith, and J. Hermanson, Phys. Rev. B **34**, 5548 (1986).

[54] L. Ley, R. A. Pollak, F. R. McFeely, S. P. Kowalczyk, and D. A. Shirley, Phys. Rev. B **9**, 600 (1974).

[55] W. Drube, D. Straub, and F. J. Himpsel, Phys. Rev. B **35**, 5563 (1987).

[56] T.-C. Chiang, J. A. Knapp, M. Aono, and D. E. Eastman, Phys. Rev. B **21**, 3513 (1980).

[57] F. Fuchs, J. Furthmüller, F. Bechstedt, M. Shishkin, and G. Kresse, Phys. Rev. B **76**, 115109 (2007).

[58] J. Paier, M. Marsman, and G. Kresse, Phys. Rev. B **78**, 121201(R) (2008).

[59] P. Carrier and S.-H. Wei, Phys. Rev. B **70**, 035212 (2004).

[60] H. W. A. M. Rompa, M. F. H. Schuurmans, and F. Williams, Phys. Rev. Lett. **52**, 675 (1984).

[61] J. M. Luttinger and W. Kohn, Phys. Rev. **97**, 869 (1955).

[62] J.-W. Luo, G. Bester, and A. Zunger, Phys. Rev. Lett. **102**, 056405 (2009).

[63] T. Kotani and M. van Schilfgaarde, Phys. Rev. B **81**, 125201 (2010).

[64] L. J. Sham and M. Schlüter, Phys. Rev. Lett. **51**, 1888 (1983).

[65] R. W. Godby, M. Schlüter, and L. J. Sham, Phys. Rev. Lett. **56**, 2415 (1986).

[66] M. Grüning, A. Marini, and A. Rubio, Phys. Rev. B **74**, 161103(R) (2006).